Waves and horizontal structures in Titan's thermosphere

I. C. F. Müller-Wodarg,[1] R. V. Yelle,[2] N. Borggren,[2] and J. H. Waite Jr.[3]

[1]   The Ion Neutral Mass Spectrometer (INMS) on board the Cassini spacecraft carried out in situ measurements of neutral gas composition above 1025 km altitude in Titan's atmosphere during its flybys in October 2004 (TA) and April 2005 (T5). Strong perturbations are present in the N_2 and CH_4 densities which we interpret as vertically propagating waves. Typical vertical wavelengths range from 170 to 360 km with density and pressure amplitudes reaching 4–12% of the background values and temperature amplitudes of 5–10 K. Amplitudes over our sampled height range, 1025 (T5) or 1176 (TA) to 1600 km, remain roughly constant, implying that the exponential increase in wave amplitudes with height due to the decrease of density is offset by damping. This finding allows us to constrain the wave periods to values in the order of hours. Estimates of wave-induced acceleration of the background thermosphere suggest that the waves we observe could deposit considerable momentum in Titan's thermosphere, thereby coupling the dynamics of the upper atmosphere with that of the middle atmosphere. In addition, we infer latitudinal structures in Titan's thermosphere with a factor of 3–4 increase of mass densities from pole to equator in the northern hemisphere. A preliminary evaluation of local time variations suggests densities and thermospheric temperatures to be largest near dusk, contradicting expectations for a thermosphere driven energetically and dynamically primarily by solar EUV. From the latitudinal density gradients we derived zonal wind speeds of around 245 ± 50 ms^{-1}, implying that Titan's thermosphere, like its stratosphere, could be superrotating. Our analyses were based on the TA and TS flybys only, and future Cassini Titan flybys could either support or invalidate our findings.

1.   Introduction

[2]   On 26 October 2004 the Cassini spacecraft carried out its first targeted close flyby of Titan. The closest approach altitude was 1174 km, enabling the first in situ measurements of Titan's upper atmosphere. On 16 April 2005, another close flyby occurred, this time approaching Titan to an altitude of 1025 km. During these flybys the Ion-Neutral Mass Spectrometer (INMS) instrument on board the spacecraft [*Waite et al.*, 2004] measured altitude profiles of neutral atmospheric constituents at an unprecedented level of detail, both in terms of species characteristics and spatial resolution. These measurements confirmed the three most abundant species in Titan's upper atmosphere to be N_2, CH_4, and H_2 and revealed a mean atmospheric temperature in the sampled region of 149 ± 3 K [*Waite et al.*, 2005; *Yelle et al.*, 2006]. This paper will investigate perturbations of the densities and derived thermospheric temperatures around their background values. We will interpret these perturbations as waves, characterize their vertical structures and discuss possible origins. In addition, we will investigate horizontal structures of densities and temperature in Titan's thermosphere and derive thermospheric wind velocities.

[3]   The first indication of waves in Titan's atmosphere came from radio occultation observations by the Voyager spacecraft in 1980, which detected scintillations in Titan's lower atmosphere that were interpreted as signatures of gravity waves [*Hinson and Tyler*, 1983; *Friedson*, 1994]. These waves were thought to be generated near the surface and to propagate meridionally at speeds of up to 2 ms^{-1}; it was proposed that they could deposit considerable amounts of momentum in Titan's atmosphere, possibly contributing towards the generation of superrotation, which was detected in Titan's stratosphere [*Hubbard et al.*, 1993; *Flasar et al.*, 2005; *Sicardy et al.*, 2006]. Further evidence for waves in Titan's atmosphere was provided by ground based observations of the occultation of 28 SGR by Titan in July 1989. Analysis of the measured light curves indicated the presence of waves between 200 and 500 km altitude which had vertical wavelengths of 5–50 km and horizontal wavelengths of 25–250 km [*Sicardy et al.*, 1999]. This was confirmed by more recent observations during the occulta-

[1]Space and Atmospheric Physics Group, Imperial College London, London, UK.
[2]Lunar and Planetary Laboratory, University of Arizona, Tucson, Arizona, USA.
[3]Center for Excellence in Analytical Mass Spectrometry, Southwest Research Institute, San Antonio, Texas, USA.

tions of Tycho stars by Titan in November 2003 [*Sicardy et al.*, 2006].

[4] The Huygens probe, which successfully landed on Titan's surface in January 2005, carried an Atmospheric Structure Instrument (HASI) which consisted, amongst other, of an accelerometer experiment, measuring the probe deceleration as it descended through Titan's atmosphere. The HASI measurements provided a continuous vertical profile of atmospheric densities between the ground and around 1500 km altitude, from which pressures and temperatures have been inferred [*Fulchignoni et al.*, 2005]. Wave-like perturbations are present in these temperature profiles, which above 500 km altitude reach amplitudes of around 15 K and vertical wavelengths of around 100 km. This constitutes strong evidence for waves in Titan's atmosphere propagating upward from the lower atmosphere to thermospheric heights.

[5] The observations of waves in Titan's atmosphere raise the question of whether an understanding of global winds and temperatures on Titan may require knowledge of waves as important sources of momentum and energy. A computational study by *Tokano and Neubauer* [2002], using a General Circulation Model of Titan's lower atmosphere, investigated the propagation of waves in Titan's stratosphere which are generated by Saturn's gravitational field and the ellipticity of Titan's orbit. These calculations suggested the presence of a global scale eastward propagating wave of longitudinal wave number 2 and diurnal frequency which deposited important amounts of momentum into the background atmosphere, possibly contributing towards Titan's superrotation. In a more recent computational study by *Strobel* [2006], the problem was investigated for the entire height range from the ground to the thermosphere, using a one-dimensional (1-D) perturbation model. These calculations suggested that waves forced by Saturn's gravitational field reach saturation amplitudes near 500 km altitude, where vertical wavelengths become $100-150$ km. Their dissipation according to these calculations deposits thermal energy at a rate of 10^{-9} erg cm^{-3}s^{-1} between 500 and 900 km altitude, which is of similar magnitude as solar heating rates in the region [*Müller-Wodarg et al.*, 2000]. Many uncertainties govern these theoretical calculations, in particular the exact nature of the background winds in Titan's atmosphere, which can severely affect the vertical propagation.

[6] In the following, we will report on the in situ detection of waves in Titan's thermosphere above 1025 km altitude by the Cassini Ion-Neutral Mass Spectrometer (INMS). In section 2 we will describe the observations and characterize the waves in composition and temperature, section 3 will investigate wave periods and discuss the possible wave effects on the background atmosphere in terms of momentum and energy deposition. In section 4 we will infer horizontal structures in Titan's thermosphere and estimate zonal wind speeds. Section 5 will discuss our results and present concluding thoughts.

2. Observations and Modeling
2.1. INMS Instrument

[7] The Ion Neutral Mass Spectrometer (INMS) instrument on board the Cassini spacecraft directly samples neutral and ionized molecules in Titan's upper atmosphere, allowing us to identify species within a mass-to-charge range of $1-99$ Daltons and measure their densities [*Waite et al.*, 2004]. The INMS instrument can operate in three modes which are sensitive to ions, reactive neutrals and nonreactive neutrals, but in this study we only use data taken in the Closed Source Neutral (CSN) mode which is sensitive to nonreactive neutrals such as N_2, CH_4, and H_2. The data reduction technique for converting raw instrument counts and mass spectra into particle densities is discussed by *Yelle et al.* [2006].

2.2. Titan Flyby Trajectories

[8] The observations discussed here were acquired by the INMS instrument during two of Cassini's close flybys of Titan on 24 October 2004 and 16 April 2005, which in the following we will refer to as "TA" and "T5," respectively. In this study we consider only data taken below 1600 km altitude, over a window of roughly ±5 min around closest approach. In the following we will briefly describe the geometry of these flybys with respect to Titan.

[9] The latitude and local time coverage during TA and T5 are illustrated in Figure 1. Inbound legs are shown as blue (black) lines (solid), outbound are red/gray (dashed). During TA the spacecraft trajectory below 1600 km passed from 28°N (inbound) to 41°N (outbound) and Titan local times of 15 to 19 hours solar local time (SLT), with the closest approach (1174 km) occurring near 38.5°N at 1645 hours SLT. During T5, the trajectory below 1600 km passed from 62.3°N at 1717 hours to 48.8°N at 0214 hours SLT with closest approach (1026.5 km) at 74.0°N and 2315 hours SLT. So, closest approach to Titan during TA occurred in the northern midlatitude dusk sector and during T5 at northern (winter) polar latitudes near midnight.

[10] It is of interest to note that the range of longitudes (local times) sampled during T5 is larger than during TA. While the ground track distances covered at both flybys relative to Titan's surface are very similar, longitudinal grid points are spaced closer together at polar latitudes, hence giving a larger range of longitudes (local times) sampled within the same ground track distance. This geometric effect can also be seen in Figure 1. At both flybys, trajectories were such that the longitude ranges were larger than latitude ranges. During TA the ratio of sampled longitude to latitude ranges below 1600 km is around 4.3, at T5 it is around 5.0. Assuming an average spacecraft velocity of 6 km s^{-1}, the horizontal distance traveled within our observation window along the trajectory is around 3600 km, while vertical distance (altitude) covered relative to Titan's surface is less than 600 km, a factor of 6 smaller.

2.3. Density Observations and Modeling

[11] Figure 2 shows profiles of observed N_2 and CH_4 densities during TA and T5 plotted versus spacecraft altitude. Blue (black) and red (gray) symbols denote inbound and outbound densities, respectively. A detailed discussion of the TA profiles was presented by *Yelle et al.* [2006]. The figure shows that there are significant differences in the densities measured on inbound and outbound legs for both N_2 and CH_4 as well as an overall difference between TA and T5, with T5 densities at a given altitude being systematically smaller by roughly a factor of 2. This difference
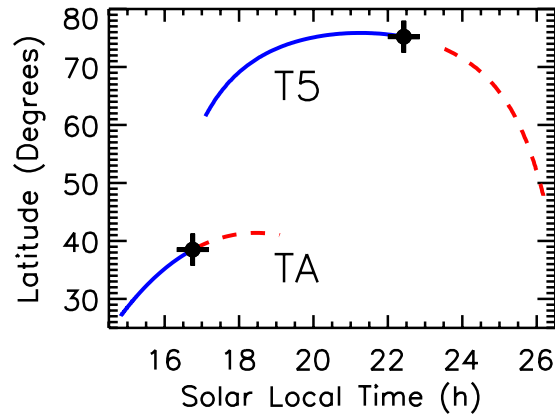
Figure 1. Trajectories of the Cassini TA and T5 flybys on Oct 26, 2004 and Apr 16, 2005, respectively, shown in terms of geographic latitude and local solar time on Titan. Only the paths of Cassini below 1600 km altitude are shown. Solid (blue/black) lines denote the inbound path, dashed (red/gray) are outbound legs. The point of closest approach to Titan is marked with a cross.

between TA and T5 densities will be discussed in detail in section 4.

[12] Similar to the study by *Yelle et al.* [2006], we use a one-dimensional diffusive equilibrium model to obtain theoretical best fits to the observed density profiles. These are shown as green (black) lines in Figure 2. The three-dimensional implementation of this model was described by *Müller-Wodarg and Yelle* [2002], but here we set the wind advection terms to zero and furthermore do not calculate the thermal structure self-consistently. We solve the vertical continuity equation by explicit time integration, calculating self-consistently the molecular and eddy diffusion velocities for both N_2 and CH_4. Chemical reactions are not considered. At the top boundary (near 1600 km) we assume diffusive equilibrium and include no escape processes. The model reaches steady state after typically one third of a Titan rotation (around 5 hours). The molecular diffusion coefficients for N_2 and CH_4 are obtained from *Mason and Marrero* [1970].

[13] The free parameters in our calculations are temperatures, the eddy diffusion coefficient and lower boundary densities. To first order, we adjust temperatures to fit the measured N_2 profiles and the eddy coefficient to fit CH_4 densities. Our assumed lower boundary mass densities are $\rho = 6.60 \times 10^{-14}$ g cm^{-3} at 1150 km altitude for TA and $\rho = 1.69 \times 10^{-13}$ g cm^{-3} at 1029 km altitude for T5. Mole fractions of CH_4 at the lower boundary are set to 2.6% for both flybys.

[14] We obtain best fits to the CH_4 densities by assuming eddy diffusion coefficients of $K = 3.5 \times 10^9$ cm^{2}s^{-1} for TA and $K = 4.0 \times 10^9$ cm^{2}s^{-1} for T5, both of which are assumed constant with altitude. These values are larger than those derived by *Smith et al.* [1982] and *Strobel et al.* [1992] from Voyager 2 measurements of (0.4–2.6) × 10^9 cm^{2}s^{-1} and up to 2 orders of magnitude larger than eddy coefficients on other planets. As pointed out by *Yelle et al.* [2006], these values may not represent atmospheric mixing alone, but could include a contribution from CH_4

escape. If CH_4 escape does occur on Titan, it will reduce the eddy coefficient that is needed to fit observed CH_4 densities. This ambiguity, however, does not affect the current study.

[15] Best fits to the observed N_2 densities over the entire altitude range are obtained by assuming isothermal conditions with temperatures of $T_{TA} = 149$ K and $T_{T5} = 155$ K at TA and T5, respectively; however, T5 measurements extend 150 km deeper into the atmosphere. In order to examine the sensitivity of temperatures to the altitude range of the fits, we also ran our model to fit T5 observations only in the altitude range overlapping with that of TA observations, 1174–1600 km. For the reduced altitude range we derived an isothermal temperature at T5 of $T'_{T5} = 153$ K. This suggests the possibility of slightly higher temperatures below 1175 km, but further constraints are necessary to support this. Thus differences in upper atmosphere temperatures between the two flybys, if real, appear relatively small. The inferred exospheric temperatures are in reasonable agreement with those derived from the reanalyzed Voyager 1 UVS occultation measurements of 153 K (158 K) at ingress (egress) [*Vervack et al.*, 2004].

2.4. Density Perturbations

[16] In the following, we will discuss perturbations in the density measurements. In order to separate the perturbations
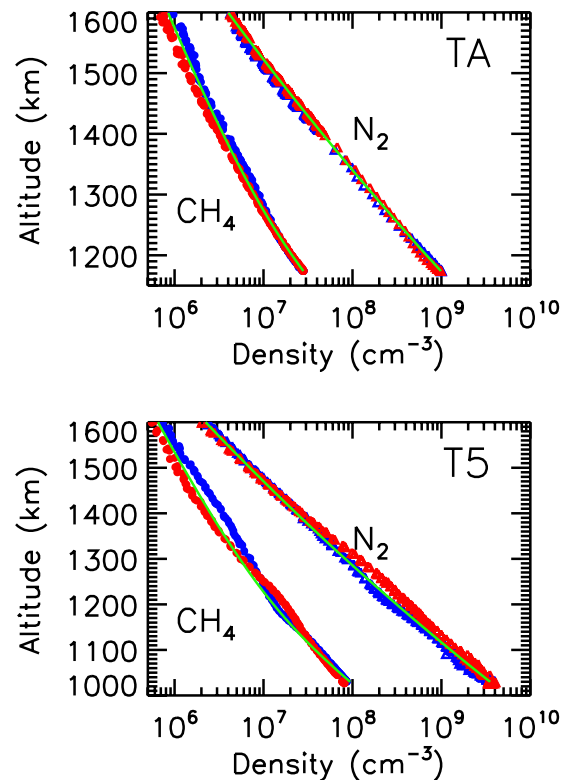

Figure 2. Nitrogen and methane densities in Titan's thermosphere, as observed by the INMS instrument during Cassini's TA and T5 flybys on Oct 26, 2004 and Apr 16, 2005, respectively. Blue (black) symbols denote densities along the inbound trajectory, red (gray) symbols are outbound. Green (black) solid lines are isothermal diffusive equilibrium distributions, as calculated by a one-dimensional model, as described in Section 2.3.
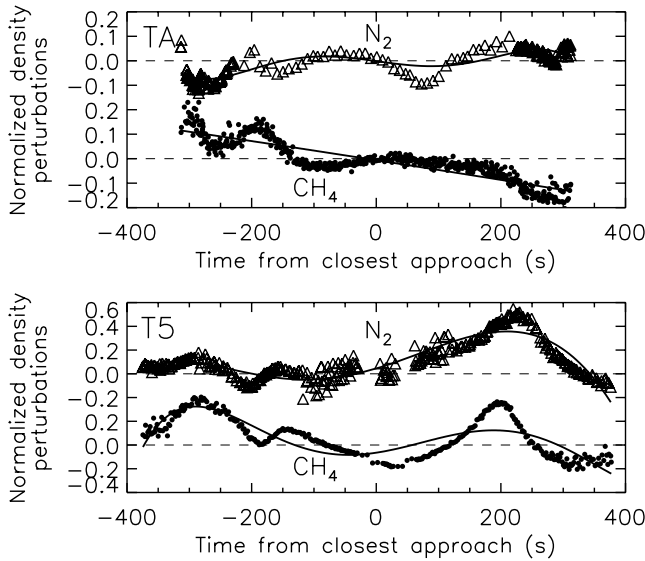
Figure 3. Normalized N_2 and CH_4 density perturbations for TA and T5 flybys on Oct 26, 2004 and Apr 16, 2005, respectively. Values are plotted versus time from closest approach to Titan (in seconds). The perturbations are calculated as $\varepsilon_i = (n_i - \bar{n}_i)/\bar{n}_i$, n_i being the measured densities and $\bar{n}_i$ the diffusive equilibrium distribution. Solid lines are polynomial fits to the measurements. They may represent background trends in the atmosphere.

from background densities we subtracted measured gas density values n_i from the modeled diffusive equilibrium distribution densities $\bar{n}_i$ (green/black curves in Figure 2, see section 2.3). Figure 3 shows normalized density perturbations $\varepsilon_i = (n_i - \bar{n}_i)/\bar{n}_i$ for N_2 and CH_4 at TA and T5 flybys versus time from closest approach. The triangles denote N_2 perturbations and dots denote those of CH_4. We see in Figure 3 the presence of numerous periodic perturbations both in N_2 and CH_4. These have amplitudes in the order of 10% at TA and slightly larger at T5. Interestingly, the perturbations of both gases at any given flyby are not always in phase, particularly during the TA inbound pass (left half of the upper panel in Figure 3).

[17] In addition, general trends are present in the perturbations with spatial scales larger than the perturbations. To extract these trends, we fitted fifth degree polynomials to the data, shown in Figure 3 as solid lines. These trends are different for N_2 and CH_4, and furthermore they are larger during T5 than TA. During the flybys the spacecraft sampled not only different altitudes, but also moved horizontally (see section 2.2), whereas we assumed a uniform vertical background density profile at all times during each flyby. Therefore the trends identified in Figure 3 may represent horizontal structures in Titan's atmosphere (see also section 4). The polynomials could also represent larger-scale vertical waves, but from the observations this distinction cannot be made. Some uncertainty remains in separating the perturbations from background trends in the atmosphere since the vertical wavelengths we observe are comparable in magnitude to the sampled height range. This uncertainty would primar-

ily affect the amplitudes, while vertical wavelengths would vary by a few kilometers only.

2.4.1. Distinguishing Horizontal From Vertical Perturbations

[18] Atmospheric waves have three-dimensional structures with both horizontal (latitudinal/longitudinal) and vertical wave numbers. In our observations we sample a horizontally and vertically constrained region only, and within that region we may compare horizontal and vertical amplitudes and wavelengths of perturbations. When vertical wavelengths are smaller than the sampled height range and vertical amplitudes exceed horizontal variations, we may denote the wave as a "vertical wave." Most global-scale atmospheric wave fit into this category. On the other hand, waves with large horizontal amplitudes and wavelengths that fit within the horizontal sampled range can be denoted as "horizontal waves." One key question is whether to interpret the perturbations in Figure 3 as horizontal or vertical perturbations in the atmosphere. Since the spacecraft moved both horizontally and vertically through Titan's atmosphere, either option is possible or we may be observing a combination of both. To assess this question, we will discuss the locations of observed perturbations in Titan's atmosphere.

[19] Figure 4 shows normalized perturbations of mass density, $\Delta\rho/\rho$, during TA. Large scale trends (such as those seen in Figure 3) are extracted. The upper panel shows values versus distance traveled by the spacecraft along its trajectory (relative to the point of closest approach), while in
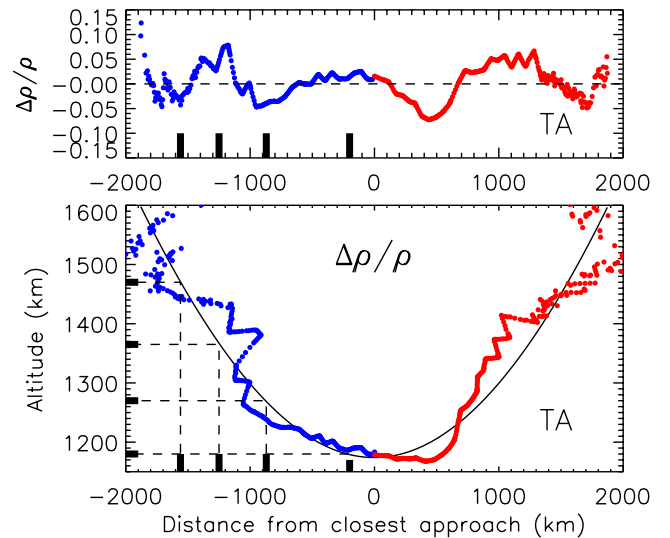

Figure 4. Normalized perturbations of mass density ($\Delta\rho/\rho$) in Titan's atmosphere, as measured by the INMS instrument on board Cassini during the TA flyby on October 26, 2004. Large scale trends have been removed from the data. The upper panel shows values versus distance from closest approach along the trajectory. In the lower panel, this curve is warped along the trajectory curve (solid line), shown versus altitude in the atmosphere and horizontal distance from closest approach. Black markers indicate the locations of extrema in the perturbation curve, mapped onto the horizontal and vertical axes. Inbound values are blue (black), outbound values are in red (gray).

the bottom panel we show the same curve warped along Cassini's trajectory in Titan's atmosphere, plotted versus altitude and horizontal distance. This view allows us to visualize the altitudes and horizontal distances at which perturbations occur and how the inbound and outbound observations relate to one another. The perpendicular distances of the markings to the trajectory line (solid) qualitatively represent the density perturbations. In the upper panel the markers along the x-axis indicate approximate positions of extrema in the inbound curve. These same locations have been drawn on the x-axis of the bottom panel and projected onto the equivalent altitudes on the y-axis. This allows us to visualize the horizontal and vertical distances in Titan's atmosphere of density maxima and minima.

[20] When comparing the distances between extrema as projected onto the altitude axis with those projected onto the horizontal distance axis, we note that their spacing is virtually uniform in altitude (at around 100 km), implying a roughly 200 km vertical wavelength. On the horizontal distance scale, spacing increases from around 300 km to almost 600 km. The horizontal wavelengths of a wave should be roughly constant, thus the characteristics described above suggest that the perturbations are primarily vertical. If densities were to have primarily horizontal perturbations in the atmosphere, their spacing on the x-axes in Figure 4 would be more uniform.

[21] Figure 4 also shows that perturbations above 1300 km correlate well between the inbound and outbound passes. This suggests that the spacecraft is sampling the same vertical region of perturbations in the atmosphere, supporting the idea that these are not localized perturbations but form part of a larger-scale phenomenon spanning over no less than 2000 km, or around 30° latitude/longitude. In summary therefore there is strong evidence that the perturbations observed in the INMS measurements are large-scale vertically propagating waves. We will therefore for the remainder of this study show them plotted versus altitude in the atmosphere. Some small-scale perturbations are also evident in Figure 4, but these will not be discussed as part of this study.

[22] Finally, we will briefly compare horizontal and vertical gradients in gas densities to the slope of the spacecraft trajectory in order to assess where the instrument might be observing horizontal rather than vertical variations in gas densities. In most cases the vertical gradients in gas density exceed horizontal gradients. For Titan, the simulations by *Müller-Wodarg et al.* [2003] found strong horizontal gradients in CH_4 abundances driven by the global circulation on Titan. In terms of magnitude, these compared well to those observed by the INMS instrument on the inbound and outbound passes of TA and T5 (see Figure 2). It can be shown that the ratios of vertical to horizontal gradients in CH_4 densities is given by $\xi = \Delta x/(H_{CH_4} \cdot \Delta X_{CH_4})$, where H_{CH_4} is the CH_4 scale height and ΔX_{CH_4} is the change in mixing ratio of CH_4 over a horizontal distance Δx. From the calculations of *Müller-Wodarg et al.* [2003] we find typical values of $\Delta X_{CH_4} \approx 0.2$ for $\Delta x \approx 2000$ km. Assuming $H_{CH_4} \approx 120$ km we obtain $\xi \approx 80$. This means that vertical gradients in CH_4 densities on Titan will exceed horizontal gradients by at least a factor of 80. For N_2 this value will be far larger since horizontal gradients of N_2 are likely to be significantly smaller than those of CH_4 [*Müller-*
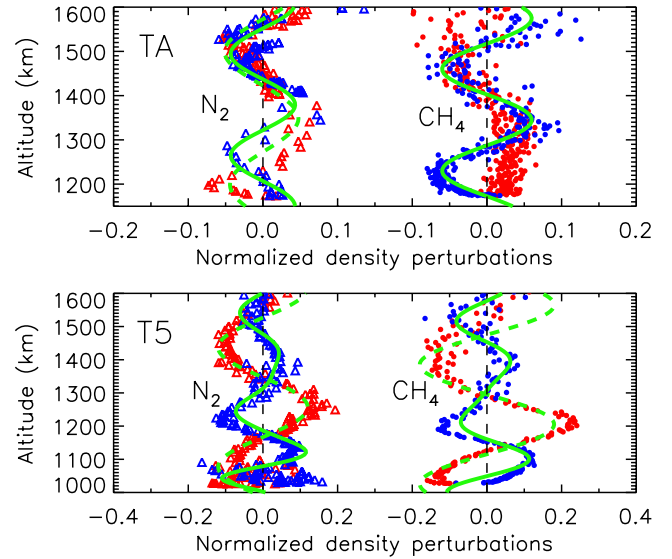

Figure 5. Normalized perturbations of N_2 (triangles) and CH_4 (dots) versus altitude in Titan's thermosphere, as measured by the Cassini INMS instrument during the TA and T5 flybys. The perturbations are relative to the diffusive equilibrium distributions of gases. Large scale trends have been extracted. Blue (black) markers denote the inbound trajectory values, red (gray) markers are outbound. Green (black) curves are spectral fits to inbound (solid) and outbound (dashed) values (see Table 1). Perturbations in mass density ρ were found to be almost identical to those in N_2.

Wodarg et al., 2003]. The Cassini spacecraft trajectory during TA and T5 had slopes with respect to Titan's surface larger than 0.1 (absolute value) down to 25 km above closest approach altitude. If the spacecraft is to encounter primarily horizontal density structures in the atmosphere, the trajectory slope needs to be smaller than ($1/80 \approx 0.013$). We found these small slopes to be reached only within 300 m altitude (50 km horizontal distance) of closest approach. Therefore local density perturbations detected by the INMS are most likely primarily due to changes in altitude than horizontal distance, despite the overall horizontal geometry of the trajectories. In our estimate of horizontal gradients we did not consider the possibility of localized sharper gradients, but those would probably only affect the smaller scale density perturbations in Figure 4.

2.4.2. Wave Characteristics

[23] Figure 5 shows perturbations of N_2 and CH_4 densities mapped versus altitude in Titan's atmosphere. In all curves, large-scale background trends have been removed as much as possible. Perturbations of ρ (shown in Figure 9 and discussed in section 2.5.3) closely resemble those of N_2 since N_2 is the principal gas throughout our sampled height regime with CH_4 mixing ratios ranging from around 2.6% near 1150 km to 25% near 1600 km (as shown in Figure 12 and discussed in section 4.2).

[24] Atmospheric perturbations are present in both flybys with amplitudes of 5–10% during TA and 10–20% during T5. The perturbations of N_2 and CH_4 densities correlate well, particularly during the TA and T5 inbound passes

Table 1. Composition Wave Properties in Titan's Thermosphere During the Cassini TA and T5 Flybys[a]

	N_2 (TA) Inbound	N_2 (TA) Outbound	CH_4 (TA) Inbound	CH_4 (TA) Outbound	N_2 (T5) Inbound	N_2 (T5) Outbound	CH_4 (T5) Inbound	CH_4 (T5) Outbound
λ_1, km	230	300	230	/	270	360	270	360
A_1	0.043	0.040	0.060	/	0.070	0.120	0.070	0.180
Φ_1, km	1380	1348	1345	/	1399	1257	1377	1205
$(1/\alpha)_1$, km	∞	∞	∞	/	∞	∞	∞	∞
λ_2, km	/	/	/	/	170	/	170	/
A_2	/	/	/	/	0.060	/	0.060	/
Φ_2, km	/	/	/	/	1305	/	1270	/
$(1/\alpha)_2$, km	/	/	/	/	330	/	330	/

[a]Each profile is fitted with up to two wave trains, denoted by indeces "1" and "2." The resulting waves are shown in Figure 5 as green (black) lines. λ denote vertical wavelengths. The normalized perturbation amplitude values A are given for altitudes $z_0 = 1175$ km and $z_0 = 1025$ km at TA and T5, respectively. Φ denote altitudes of zero phase for each wave train. The inverse vertical damping parameter values $(1/\alpha)$ are the vertical distances over which amplitudes are reduced by a factor of e. A value of ∞ denotes a wave train with constant amplitude over the sampled height range. Waves in mass density ρ were found to be almost identical to those in N_2.

(blue/black markers) and T5 outbound (red/gray markers). Regular perturbations of CH_4 are less evident in the TA outbound values, where we observe only around half the cycle of a possible wave.

[25] In order to better define the wave properties, we have applied simple fits to the density curves. For gas i the normalized perturbation $\varepsilon_i = \Delta n_i / n_i$ is expressed as

$$\varepsilon_i(z) = \sum_n A_{i,n} \cos\left(k_{i,n}(z - z_0) + \phi_{i,n}\right) \cdot e^{-\alpha_{i,n}(z - z_0)} \qquad (1)$$

where $A_{i,n}$, $k_{i,n}$ and $\phi_{i,n}$ are amplitudes, wave numbers ($k_{i,n} = 2\pi/\lambda_{i,n}$) and phases for the ith constituent, respectively, and z_0 is an (arbitrary) bottom altitude. Factors $\alpha_{i,n}$ are a measure for vertical damping, in that $1/\alpha_{i,n}$ denote the altitudes over which amplitudes decrease by a factor of e. We allow for multiple wave trains in each gas, hence the sum in above equation over n, and found reasonable fits with two wave trains or fewer. The green/black lines in Figure 5 are spectral fits to the density perturbations. Their properties are listed in Table 1. Since no clear periodicity is evident in the outbound CH_4 values during TA, no spectral fit was attempted.

[26] From Figure 5 and Table 1 we see that N_2 and CH_4 perturbations are dominated by periodicities with vertical wavelengths of 230 km at TA inbound, 300 km at TA outbound, 270 km at T5 inbound, and 360 km at T5 outbound. A second wave train with 170 km wavelength is present in the T5 inbound values of N_2. At TA, inbound and outbound N_2 amplitudes are very similar (around 4%). At T5 this is not the case, with outbound amplitudes about 1.7–2.6 times larger than inbound amplitudes. T5 inbound amplitudes have values of around 7%, a factor of 1.8 larger than TA values. The second wave trains at T5 (inbound) have a comparable amplitude of 6%.

[27] Also shown in Table 1 are altitudes of zero phase for all wave trains. In principle, these would allow us to compare the phasing between N_2 and CH_4 waves and, secondly, the phasing between the inbound and outbound values for any given gas. Since amplitudes on inbound and outbound legs differ by around 25%, we will only compare the phasing between N_2 and CH_4. At TA, the phases of inbound N_2 and CH_4 perturbations differ by 35 km, at T5 their differences are 22 km and 52 km for inbound and

outbound values, respectively. Some uncertainty is present in the TA inbound phase shifts. Owing to a counter saturation problem, the vertical resolution of N_2 measurements below 1400 km was reduced, adding some uncertainty to the values. We attempted to apply the CH_4 fit to N_2, but found an unsatisfactory match to the observations below 1250 km. While the fitted TA inbound N_2 curve therefore bears some uncertainty, it is nevertheless the best fit, based on the available information. Phase shifts between perturbations of different gases were also found in the thermosphere of Earth (N_2 and He) [*Reber et al.*, 1975] and on Venus (CO_2 and He) [*Kasprzak et al.*, 1993].

[28] Table 1 also lists the inverse values of the damping parameters, α. We obtained best fits for most curves by applying $\alpha = 0$, except for the secondary N_2 waves at T5 (inbound), for which we obtained a vertical damping height of 330 km. The implication of this is that the larger of our waves have roughly constant amplitudes over the height range that we observe. If the waves were undamped, their amplitudes should increase with altitude proportional to $(1/\sqrt{\rho})$. Over the considered height range this would imply an amplitude growth by a factor of about 45. The roughly constant amplitudes in our results imply that the growth is balanced by damping forces, such as viscosity. This is further discussed in section 3.2. We see some evidence of damping in the measured density perturbations in T5 outbound values in Figure 5 above 1450 km, but it is unclear whether this is indeed damping or the effect of background density variations.

2.5. Pressure and Temperature Perturbations
2.5.1. Reduction Technique and Errors
[29] Two important parameters which are not directly measured by the INMS instrument are atmospheric pressure and temperature. In the following we will describe the technique we use to derive these. In section 2.3 we described the calculation of diffusive equilibrium best fits to observed gas densities. In these model fits we assumed isothermal temperature values and, as a by-product of the model, we obtained vertical profiles of pressure. It should be noted that these represent values for the unperturbed background atmosphere. The pressures and temperatures we derive in the following will include perturbations of Titan's real atmosphere relative to the background values.

[30] From measurements of N_2 and CH_4 number densities we obtain mass densities ρ along the spacecraft trajectory within our considered height range where N_2 and CH_4 are principal gases in Titan's thermosphere. Since N_2 and CH_4 measurements are not carried out simultaneously we interpolate the CH_4 densities onto the N_2 measurement locations (altitudes) and calculate mass densities ρ on this common height grid. The mass densities are then used to derive vertical profiles of atmospheric pressure.

[31] For an atmosphere in hydrostatic equilibrium the change of pressure with altitude is related to the weight of the atmosphere above through the hydrostatic relation

$$dp = -\rho g \, dz \qquad (2)$$

where ρ is the mass density and g the gravity acceleration. To obtain the pressure at an altitude z, the above relation may be integrated downward from an altitude z_{top}:

$$p(z) = p_{top} + \int_{z_{top}}^{z} \rho(z')g(z')dz' \qquad (3)$$

From our INMS measurements we obtain two profiles of mass densities ρ for each flyby, one inbound and one outbound. As outlined in section 2.2, the spacecraft moves both horizontally and vertically, so density values are not sampled within a vertical column of gas. The uncertainty introduced by this is discussed in section 2.5.2.

[32] Gas densities are measured by INMS at variable vertical intervals of typically between 0.2 and 3 km. To improve accuracy in our numerical integration of equation (3) between adjacent altitude steps, we use the log-linear interpolated density value between the levels. This reduces the occurrence of any artifacts due to varying sampling resolution of measurements.

[33] The boundary condition p_{top} in equation (3) is necessary because p_{top} has a nonnegligible value at the upper boundary altitude of our integration, $z_{top} = 1600$ km. The value cannot reliably be inferred from the spacecraft data. We therefore take p_{top} from the background pressure profiles calculated with our 1-D diffusive equilibrium model (Section 2.3). For TA and T5 conditions, respectively, the upper boundary pressures we assumed are $p_{TA} = 1.003 \times 10^{-4}$ nbar and $p_{T5} = 4.095 \times 10^{-5}$ nbar. Temperatures are calculated from the derived pressures and measured densities using the ideal gas law.

[34] The derived temperature profiles are shown in Figure 6. As previously, blue (black) and red (gray) symbols denote inbound and outbound values, respectively. Strong perturbations are seen in the temperatures of Figure 6, oscillating with average amplitudes of 5–10 K around the background values of around 149 K (TA) and 155 K (T5). Both at TA and T5, perturbations of the inbound profiles have an average vertical wavelength of 200–250 km. The outbound temperatures exhibit a less periodic behavior than inbound, especially for T5. The solid lines are polynomial fits to the data which may be linked to horizontal structures in the atmosphere, which are discussed further in section 4.

[35] Also shown in Figure 6 are error bars which we calculated as follows. Each N_2 and CH_4 number density value measured by INMS has an uncertainty due to count-
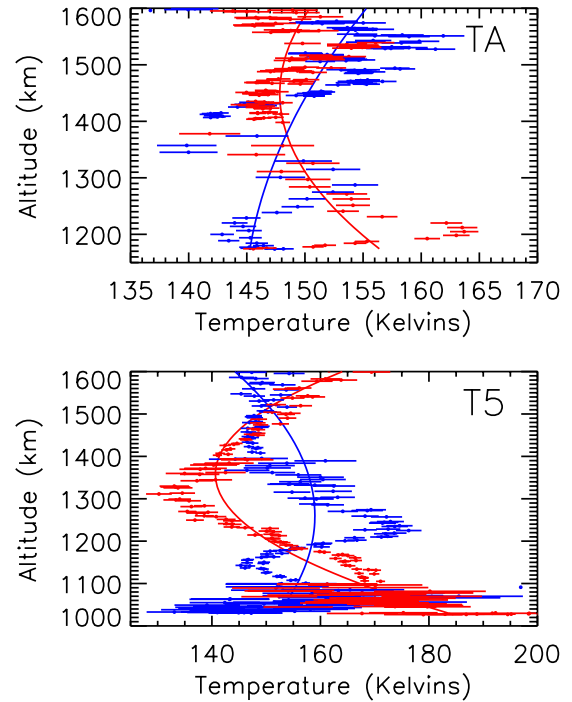

Figure 6. Temperatures in Titan's thermosphere derived from N_2 and CH_4 densities measured during the TA and T5 flybys. Blue (black) symbols denote densities along the inbound trajectory, red (gray) symbols are outbound. Also shown are derived errors. Solid curves are polynomial fits which represent larger scale background trends and are subtracted to obtain the perturbations of Figure 9.

ing statistics. Typically, these uncertainties are below 10% [*Waite et al.*, 2004] and hardly visible on the scale of Figure 2. We derived a series of 1000 pressure and temperature profiles using the technique described above, each time allowing N_2 and CH_4 number densities to vary randomly, assuming a Gaussian distribution with a standard deviation equal to the error bar. At each location, this generated 1000 different pressure and temperature values, for which we calculated the standard deviations. The average temperature uncertainties are around 1.3 K at TA and 1.6 K at T5, but larger in regions of fewer measurement points.

[36] Another uncertainty lies in our choice of upper boundary condition p_{top} when solving equation (3). This uncertainty is not included in the error bars of Figure 6, but will be illustrated in the following. Our choices of upper boundary pressures for TA and T5 (described earlier) can also be expressed in terms of temperatures and correspond to values of 149 K and 155 K, respectively. In order to illustrate the sensitivity of our derived vertical temperature profiles to the choice of these upper boundary conditions, Figure 7 shows a temperature profile for TA inbound conditions. The nominal profile (denoted by dots) assumes an upper boundary background temperature of 149 K. We recalculated temperature profiles for a range of upper boundary pressure (temperature) conditions varying by up to $\pm 10\%$ (± 15 K) with respect to the nominal value. The range of derived temperatures is illustrated in Figure 7 with error bars around the nominal profile. We see that the
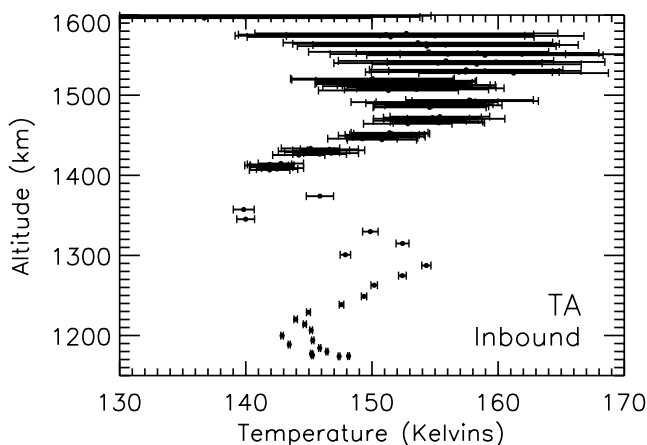
Figure 7. Temperatures in Titan's thermosphere derived from inbound density observations during the TA flyby. The figure illustrates the sensitivity to the choice of upper boundary conditions in our temperature calculations. The nominal profile assumes an upper boundary temperature of 149 K, the error bars illustrate the lower and upper ranges of temperatures derived when assuming an upper boundary temperature reduced and increased by 15 K, respectively.

measured densities at those locations are $\rho(TA) = 6.96 \times 10^{-12}$ kg/m^3 and $\rho(T5) = 3.56 \times 10^{-12}$ kg/m^3, a ratio of $\rho(TA)/\rho(T5) \approx 2$. We implemented a latitudinal density gradient in our model to satisfy this density ratio at the two locations. The resulting normalized density profile is shown in the upper panel of Figure 8. We only show densities within the latitude regime of the TA trajectory and normalized values to the density at the latitude of closest approach ("CA"). We found the latitudinal gradient of normalized densities at any given height level to be virtually invariant with altitude within our height regime. The upper panel in Figure 8 is therefore representative of latitudinal density structures between around 1000 and 1600 km altitude. We constrained our latitudinal density gradient implemented in the model only with two measurement points, and any real latitudinal structure in Titan's thermosphere may differ from this simplistic profile. A more detailed analysis of latitudinal density structures is presented in section 4.

[40] The temperatures that we derived from this atmosphere model are shown in the lower panel of Figure 8 as solid (inbound) and dashed (outbound) lines alongside the known model temperature values (dotted line). While the assumed model temperature was isothermal and hence identical inbound and outbound, large discrepancies are apparent in the derived values, especially in the inbound profile and strongest at closest approach, where temper-
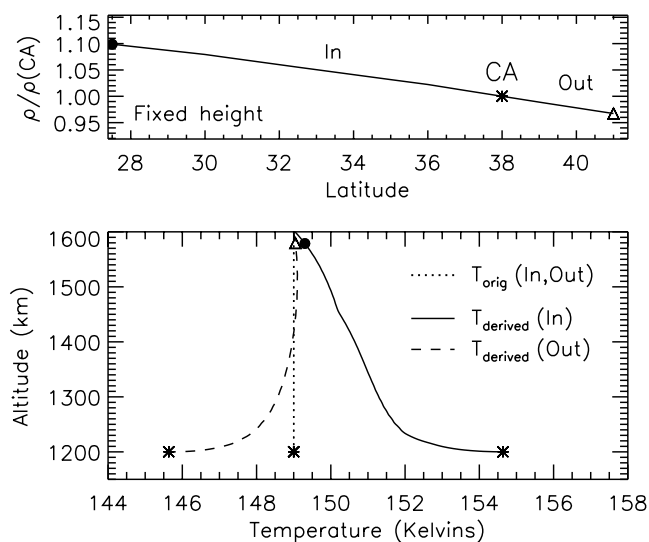
temperatures above 1400 km are sensitive to the choice of upper boundary condition, but at lower altitude it matters little within the range we assumed.

2.5.2. Effects of Horizontal Structures on Derived Temperatures

[37] Our derivation of temperatures, described above, relies upon calculating pressures from the density observations. To derive pressures at a specific location we need to sum up the weight of the atmosphere above. In our analysis we take the density values above a location of interest from observations made at higher altitudes along the spacecraft trajectory. As outlined in section 2.2, Cassini's trajectories during the flybys cover around 6 times more distance horizontally than vertically with respect to Titan. If horizontal changes of densities are present in Titan's atmosphere, the densities along the spacecraft trajectory will not be the same as those inside a column above any specific location. Horizontal structures in the atmosphere will therefore affect the derived pressures and temperatures.

[38] To assess the effect of this, we used a 2-D (latitude-height) version of our diffusion model described in section 2.3, in which we imposed a latitudinal density structure. We then generated synthetic spacecraft measurements along the TA orbit (projected into the latitudinal plane only) and used these to derive temperatures in the same way as described above. These are compared to the model's known isothermal temperature values (T = 149 K) in Figure 8.

[39] In order to estimate a realistic latitudinal density gradient in Titan's atmosphere we compare the measured densities between the TA and T5 flybys. As can be seen from Figure 1, the outbound TA and inbound T5 trajectories sample a similar local time regime. Both trajectories in the local time/altitude domain intersect one another at 1800 hours SLT/1316 km. At this point, Cassini sampled the atmosphere at same altitudes and local times, but different latitudes with values of 41.2°N (TA) and 69.1°N (T5). The

Figure 8. Illustration of the effects of horizontal composition structure on temperatures derived by the method described in Section 2.5. The upper panel shows density versus latitude at fixed altitude, normalized to the value at closest approach (CA), as specified in our 2-D synthetic isothermal atmosphere. The latitude variation is consistent with that observed during the TA and T5 flybys. The bottom panel shows temperatures retrieved from the synthetic atmosphere by flying the TA trajectory through it. The correct temperatures (T_{orig}) are shown as the dotted line, derived inbound and outbound values ($T_{derived}$) are shown as solid and dashed lines. Note the large discrepancies of temperatures derived along the inbound and outbound legs, particularly at closest approach. See text for details.
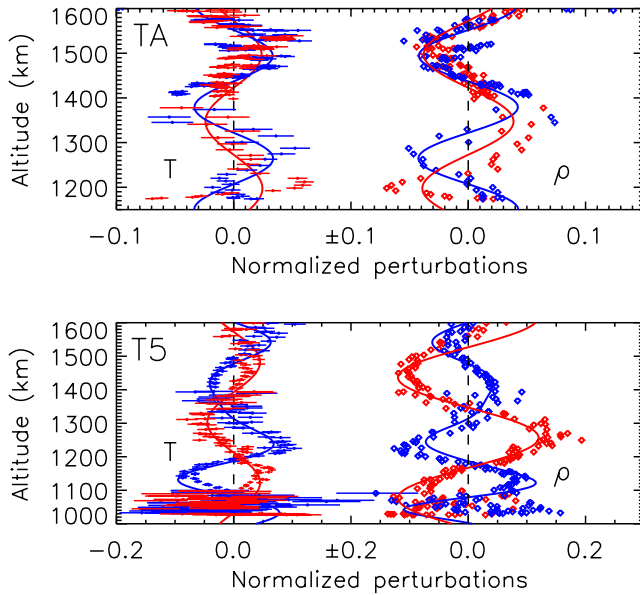
Figure 9. Normalized perturbations of temperature and mass density (ρ) in Titan's thermosphere as derived from N_2 and CH_4 densities measured during the TA and T5 flybys. Blue (black) symbols denote values along the inbound trajectory, red (gray) symbols are outbound. Also shown are derived temperature errors. Solid curves are spectral fits which for the temperatures have the properties listed in Table 2 and for ρ have the properties of N_2 in Table 1.

atures derived along the inbound and outbound legs differ by up to 9 K.

[41] What these simulations illustrate, despite their simple assumptions, is that the derived temperatures are sensitive to horizontal density variations in the atmosphere. The presence of horizontal density variations violates the implicit assumptions of equation (3) since densities sampled along the spacecraft trajectory are not identical to those in the column above the location of interest. We see from this simulation that the error in derived temperatures is most significant where horizontal composition changes are largest, and in addition it maximizes towards lower altitudes, where the integrated effect is largest.

[42] As can be seen in Figure 6, the inbound and outbound temperatures derived from INMS measurements during T5 tend to diverge near closest approach, the point at which the real temperature values should be identical inbound and outbound. At TA, they differ by up to 20 K near 1200 km altitude. The regions sampled inbound and outbound during TA at 1200 km altitude lie around 1000 km apart (see also Figure 4), and it is unlikely that this strong horizontal temperature gradient of around 0.02 K/km is real. Instead, we believe it is related to our technique of deriving the temperatures. This effect is in agreement with the simulations in Figure 8 and evidence for horizontal variations in atmospheric density, in particular the major gas N_2. We will further discuss horizontal structures in Titan's atmosphere in section 4.

2.5.3. Wave Characteristics

[43] The temperatures of Figure 6 are in the following examined closer through a spectral decomposition. In order

to separate the perturbations from any background trends, we fit polynomial curves to the temperatures, shown as solid lines in Figure 6. We calculated the normalized perturbations of temperature as $\eta(z) = (T(z) - T_0)/T_0$, where $T(z)$ are derived temperature values at a given altitude z as shown in Figure 6 minus the background trend value and T_0 are the isothermal background values of $T_0 = 149$ K (TA) and $T_0 = 155$ K (T5).

[44] Figure 9 shows the normalized temperature perturbations during the TA and T5 flybys versus altitude in Titan's atmosphere. Also shown are vertical profiles of normalized mass density perturbations, $\Delta\rho/\rho$, which are the same as shown in Figure 4 with background trends removed, but mapped versus altitude. Note that the background density and temperature trends were derived independently from one another. Superimposed as solid lines are simple spectral fits to the curves, which we carried out in manner identical to that described for the densities (section 2.4.2). The spectral characteristics of the temperature fits are summarized in Table 2, whereas the characteristics of the mass density fits are identical to those of N_2 in Table 1.

[45] It is of interest to compare the temperature and density perturbations in Figure 9. From the relation $\rho = pM/kT$, where p, M, k and T are the pressure, mean molecular mass, Boltzmann constant and temperature, respectively, it follows that

$$\frac{\delta\rho}{\rho} = \frac{\delta M}{M} + \frac{\delta p}{p} - \frac{\delta T}{T} \quad (4)$$

From INMS measurements of mean molecular mass and derived pressure profiles (not shown) we find that $\delta M/M \approx 0.01$, $\delta p/p \approx 10^{-4}$ and we see from Figure 9 that $\delta T/T \approx 0.1$ and $\delta\rho/\rho \approx 0.1$. Since the first two terms on the right side of equation 4 are negligible it follows that to first approximation $\delta\rho/\rho \approx -\delta T/T$, or that perturbations in temperature and density are in antiphase. This is largely confirmed by the values in Figure 9.

[46] As a result, the properties of our temperature wave fits (Table 2) are almost identical to those of composition

Table 2. Temperature Wave Properties in Titan's Thermosphere During the Cassini TA and T5 Flybys[a]

	TA Inbound	TA Outbound	T5 Inbound	T5 Outbound
λ_1, km	230	300	270	360
A_1, K	5.1	3.7	8.5	7.0
A_1 (normalized)	0.034	0.025	0.055	0.045
Φ_1, km	1265	1198	1264	1123
$(1/\alpha)_1$, km	∞	∞	∞	∞
λ_2, km	/	/	170	/
A_2, K	/	/	9.3	/
A_2 (normalized)	/	/	0.060	/
Φ_2, km	/	/	1220	/
$(1/\alpha)_2$, km	/	/	330	/

[a]Each profile is fitted with up to two wave trains, denoted by indeces "1" and "2." The resulting waves are shown in Figure 9 as solid lines. λ denote vertical wavelengths. Both absolute and normalized temperature amplitudes, A, are given. The amplitudes are given as undamped values. Φ denote altitudes of zero phase for each wave train. The inverse vertical damping parameter values $(1/\alpha)$ are the vertical distances over which amplitudes are reduced by a factor of e. A value of ∞ denotes a wave train with constant amplitude over the sampled height range.
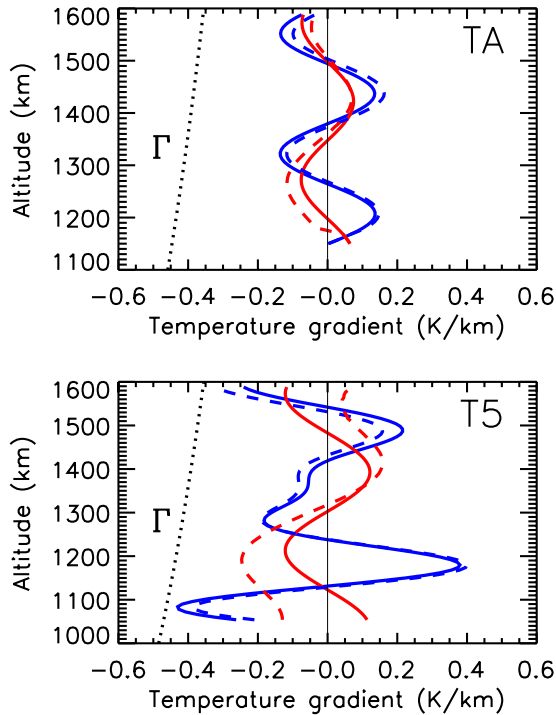
Figure 10. Vertical temperature gradients during the TA and T5 flybys. Inbound values are blue (black), outbound values are red (gray). Solid lines are gradients for the perturbations only, whereas dashed lines include the background trends of the atmosphere (solid lines in Figure 6). Also shown is the negative of the adiabatic lapse rate (dotted).

(Table 1), except for the phases and amplitudes. Individual temperature wave train amplitudes vary from around 4 K (TA outbound) to 9 K (T5 inbound) and vertical wavelengths as for composition range from 170 to 360 km. Some discrepancies are apparent in Figure 9 between the fits and the measurements, particularly at low altitudes. These are primarily due to the uncertainties in deriving temperatures discussed previously (sections 2.5.1 and 2.5.2).

[47] It is of interest also to examine vertical temperature gradients in Titan's thermosphere. We derived these from the fitted curves in Figure 9 and show them in Figure 10. As before, inbound values are blue (black) and outbound values are red (gray). Solid lines are gradients for the perturbations only, whereas dashed lines include the background trends of the atmosphere (solid lines in Figure 6). Also shown is the negative of the adiabatic lapse rate, $\Gamma = -g/c_p$, which represents a natural limit for vertical temperature gradients. The figure shows that temperature gradients are consistently larger (less negative) than the adiabatic lapse rate, so no instabilities appear to be present in the atmosphere as a result of the perturbations. Despite the limitations in deriving temperatures from the density observations, as described in section 2.5.1, the behavior of temperature gradients suggests that the observed perturbations are physically plausible. When calculating temperature gradients directly from the inferred values instead of the fits, values fluctuate considerably and may at individual altitude points exceed the adiabatic limit. However, these are largely related to the uncertainties in derived temperatures expressed by the error bars in Figures 6 and 9 and probably do not represent actual temperature gradients due to larger-scale waves we observed.

3. Effects of Waves

3.1. Wave Periods

[48] Conservation of momentum requires the amplitudes of upward propagating waves in an atmosphere to increase with altitude at a rate proportional to $1/\sqrt{\rho(z)}$ ($\rho(z)$ being the mass density of the ambient atmosphere). In the upper atmosphere molecular viscosity and thermal conduction become important processes which act to damp vertically propagating waves, eventually causing complete dissipation of the wave. The wave dissipation is accompanied by the deposition of wave momentum and energy into the background atmosphere, potentially affecting the wind speeds and redistributing energy in the atmosphere. Upward propagating waves may thus play an important role in controlling the dynamics of Titan's thermosphere. This is known to happen on Earth and thought to be of crucial importance also on Venus, helping to slow down day-to-night circulation and maintain the cold nighttime thermospheric temperatures. We will in the following examine the role of waves in Titan's thermosphere with respect to dynamics and energetics.

[49] As pointed out in section 2.4.2, wave amplitudes should in the absence of any damping have increased by a factor of around 45 within our altitude range. The waves we found in density (Figure 5) and temperature (Figure 9) however to first order have constant amplitudes. We may therefore assume that damping balances the $1/\sqrt{\rho}$ amplitude increase in our observations. When considering molecular viscosity and conduction to be the key damping processes, it can be shown that the growth of the wave is balanced by damping when

$$\frac{(\nu + \kappa)k^3}{\omega} = \frac{1}{H} \qquad (5)$$

where H is the total density scale height, ω the wave frequency, ν and κ are the kinematic viscosity and thermal diffusivity, respectively, and $k^2 = k_h^2 + k_z^2$ is the total wave number (k_h and k_z being the horizontal and vertical wave numbers, respectively). We calculate the kinematic viscosity $\nu = \mu/\rho$ by assuming $\mu = 1 \times 10^{-5}$ kg (m s)$^{-1}$ and thermal diffusivity $\kappa = \Lambda/(\rho\,c_p)$ by assuming $\Lambda = 27.21 \times 10^{-5}\,T^{0.8}$ J (m K s)$^{-1}$ and $c_p \approx 1450$ J (kg K)$^{-1}$. We obtain values for H and $k_z = 2\pi/\lambda_z$ (Table 2) from our observations. If we assume global scale waves with horizontal wavelengths of the order of a Titan Radius, $k_h \ll k_z$ and $k \approx k_z$. This allows us to use relation (5) to calculate ω and thereby the wave periods, $T_\omega = 2\pi/\omega$.

[50] We calculated T_ω for three wavelengths representative of our observations, $\lambda_z = 170$ km, $\lambda_z = 270$ km, and $\lambda_z = 360$ km, and obtain $T_\omega \approx 4$ hours, 15 hours, and 35 hours, respectively, near 1030 km altitude. These values are the periods that a wave damped by viscosity and thermal conduction has at the altitude where amplitudes reach their saturation values. Since damping by molecular viscosity and conduction increase exponentially with altitude, the region where amplitude increase and damping balance can only

extend over a few scale heights ($H = 70-90$ km at the heights of interest). Since the amplitudes we observe are roughly constant with altitude, it is likely that we are sampling the altitudes where the balance of equation (5) holds and wave amplitudes have reached their saturation values. The kinematic viscosity and thermal diffusivity coefficients used in equation (5) depend on the density ρ and values for T_ω hence decrease exponentially with altitude. The above T_ω values can therefore be regarded as order of magnitude estimates only and as upper limits to the wave periods.

[51] Calculations by *Strobel* [2006] have suggested that diurnal gravitational tides reach thermospheric altitudes, raising the question of whether we could be observing the diurnal gravitational tides. To assess this, we invert the earlier problem and ask at what critical density ρ_c and altitude a gravity wave with diurnal period and wavelengths within our observed ranges would reach their saturation amplitude. Using equation (5) we calculate values of $\rho_c \approx 1.8 \times 10^{-8}$, 4.5×10^{-9} and 1.9×10^{-9} kg m^{-3} for wavelengths $\lambda_z = 170$, 270 and 360 km, respectively. Using an updated version of the engineering model of Titan's atmosphere by *Yelle et al.* [1997] which takes into account the latest observations, these densities correspond to altitudes of around 790, 870 and 930 km, respectively. Since equation (5) makes a number of simplifying assumptions, these values are again first order estimates only, but they are similar to the values derived by *Strobel* [2006] for gravitational diurnal tides (500–900 km, depending on the assumed zonal wind profiles). The important implication of our results is that viscosity and conduction effectively filter out long period waves in the lower thermosphere, allowing only those with periods of up to tens of hours to reach altitudes above ~1000 km.

[52] The vertical wavelengths we observed are around twice as large as those measured by the HASI instrument on board the Huygens probe [*Fulchignoni et al.*, 2005]. The presence of strong horizontal winds can Doppler-shift horizontal wavenumbers, which via the dispersion relation will change vertical wavelengths. The differences in vertical wavelength between our observations and those by HASI may therefore be related to the presence of strong horizontal background winds. In addition, the HASI observations were made near equatorial latitudes (~9°S). It is therefore inconclusive whether or not we are observing the same families of waves as HASI. Note also that above calculated wave periods do not consider effects of background horizontal winds, which would doppler-shift the results, adding uncertainties to our results which can only be reduced when better constraints are available for the dynamics in Titan's thermosphere.

[53] Timescales for vertical transport by eddy mixing in Titan's thermosphere, assuming an eddy coefficient of $K = 4 \times 10^9$ cm^{2}s^{-1}, are of the order of several hours. Above the homopause, located near 1200 km on Titan, vertical transport due to molecular diffusion becomes dominant, with time scales reaching from hours down to seconds near 1600 km. Assuming wave periods of several hours, the observed waves will probably be inefficient in mixing species in Titan's upper atmosphere. However, the waves' contribution toward transport of species may be indirect through the momentum they deposit in Titan's atmosphere, which is examined in the following.

3.2. Mean Flow Acceleration

[54] We will in the following estimate the amount of momentum that dissipating waves deposit in Titan's upper atmosphere and compare it to other accelerations, such as those driven by pressure gradients. By assuming that viscosity and conductivity balance the exponential growth of wave amplitude in the atmosphere, we can derive an expression for the momentum deposited by the damped waves into the background atmosphere. The horizontal acceleration by waves in the atmosphere is given by

$$a_h = \frac{1}{2} \frac{k_h}{k_z(k_h^2 + k_z^2)} \frac{N^2}{H} \qquad (6)$$

where N is the Brunt-Väisälä frequency, which in Titan's thermosphere has a value of $N \approx 1.2 \times 10^{-3}$ s^{-1}. We may express the horizontal wavelength as a function of s, the horizontal wave number index, such that $\lambda_h = (2\pi R_T)/s$, where $R_T = R_0 + z$, R_0 being Titan's solid body radius and z the altitude.

[55] As shown by *Tokano and Neubauer* [2002], the radial tide driven by Saturn's gravitational field generated a global wave in Titan's atmosphere of horizontal wave number $s = 2$ and diurnal period. If we assume $s \geq 2$ in equation (6) and vertical wavelengths of $\lambda_z \approx 170$, 270 and 360 km, we obtain horizontal accelerations of $a_h \geq 3.0 \times 10^{-3}$, 1.4×10^{-2} and 3.2×10^{-2} ms^{-2}, respectively. As can be seen from equation (6), waves with larger vertical wavelengths induce stronger acceleration. These values are proportional to s, so smaller horizontal wavelengths (larger s) will increase the associated a_h.

[56] How do these wave-induced accelerations compare with those driven by pressure gradients due to solar heating in the thermosphere? *Müller-Wodarg et al.* [2000] used a General Circulation Model (GCM) to calculate the global structure of Titan's thermosphere driven by solar EUV heating. Their model self-consistently calculated accelerations in the thermosphere under the influence of all processes of momentum and energy redistribution, and they found typical horizontal accelerations near 1300 km altitude at mid latitudes of around 3×10^{-3} m s^{-2}. This value is similar in magnitude or smaller than the wave accelerations derived above. At lower altitude, near 1100 km, pressure accelerations driven by solar heating were found to be much smaller, in the order of 5×10^{-4} m s^{-2}.

[57] As previously, our estimates of wave-induced accelerations should be seen as order of magnitude estimates only. Our results however suggest the possibility of waves we observe being potentially capable of depositing considerable amounts of momentum in Titan's middle and upper atmosphere which are comparable to or larger than accelerations driven by solar EUV heating. This is particularly true for the lower thermosphere, where solar EUV heating is negligible as a source of momentum. If waves deposit momentum between 500 and 1100 km altitude, this will most likely affect thermospheric dynamics due to the strong vertical coupling from viscosity. Using their Titan Thermosphere General Circulation Model, *Müller-Wodarg et al.* [2000] showed that zonal jets imposed as lower boundary condition at 600 km would cause the entire thermosphere to be accelerated from below. The dynamics of Titan's ther-

mosphere may hence considerably be affected by upward propagating waves. The calculations of *Müller-Wodarg and Yelle* [2002] and *Müller-Wodarg et al.* [2003] showed the important role that solar driven global dynamics play in redistributing constituents in Titan's thermosphere. Through their potential influence on the global dynamics, waves may hence play a key role not only in understanding global dynamics, but also in understanding the composition of Titan's thermosphere.

3.3. Wave Heating

[58] Waves not only carry momentum into the upper atmosphere but may also affect its energy balance. Undamped waves carry an energy flux which is given by the product of the energy density and the vertical group velocity. When waves are damped, they either deposit their energy locally and thereby ultimately add to the thermal energy of the region, or their mixing effect may increase the turbulent diffusion of energy, leading possibly to a local loss of energy, despite the fact that the total energy change always has to be positive. The balance of these processes has been discussed for the case of Jupiter's thermosphere in an attempt to understand how gravity waves observed by the Galileo probe affects its thermal balance [*Young et al.*, 1997; *Matcheva and Strobel*, 1999; *Hickey et al.*, 2000]. These studies found that heating rates were very sensitive to the wave characteristics, and it must be emphasized that considerable simplifications went into those calculations, as discussed by *Yelle and Miller* [2004]. It is still unclear to what extent gravity waves heat Jupiter's thermosphere, and we can in the following give simple estimates only of whether wave heating matters on Titan.

[59] In order to estimate the maximum heat flux F_{max} that an unattenuated wave can carry in an atmosphere at the point where maximum amplitudes are reached, *Yelle and Miller* [2004] extended an expression originally derived by *Strobel* [2002] and found that

$$F_{max} = 1.35 \, g \frac{\gamma - 1}{\gamma} \left(\mu + \frac{\Lambda}{c_p} \right) \tag{7}$$

where g is gravity acceleration, $\gamma \approx 1.4$ is the ratio of specific heats, and μ and Λ are the coefficients of molecular viscosity and thermal conduction (given in section 3.1). For Titan's thermosphere near 1200 km altitude, $F_{max} \approx 5 \times 10^{-6}$ Wm^{-2}. Note that this quantity is an upper limit to the amount of energy that can be carried by waves through an atmosphere and dependent only upon the atmosphere properties. Solar EUV heating rates in Titan's thermosphere range from $(8-16) \times 10^{-6}$ Wm^{-2} and are of similar magnitude.

[60] To estimate the amount of energy carried by specific gravity waves, *Matcheva and Strobel* [1999] derived an expression for the work done by pressure forces in an upward propagating gravity wave as

$$|F_z^w| \leq \frac{1}{2} \rho_0 \omega \frac{k_z}{k_h^2} W_0^2 \tag{8}$$

where ρ is the mass density, ω the wave frequency, k_z and k_h its horizontal and vertical wave number, respectively, and

W_0 is the vertical wind amplitude, which is related to temperature perturbation amplitudes by $W_0 = \omega \, g/N^2 \, (\Delta T/T)$. Assuming $\rho \approx 1 \times 10^{-11}$ kg m^{-3} (at 1200 km), $\omega \approx 10^{-4}$ s^{-1} and vertical and horizontal wavelengths of 170 km and 1200 km (corresponding to $s = 2$), respectively, we obtain for the waves we observe an upper limit of $F_z^w \leq 2 \times 10^{-6}$ Wm^{-2}. This value is similar in magnitude to the upper limit F_{max} derived above and to solar EUV heating rates in Titan's thermosphere.

[61] Since the upper limit to the energy carried by the wave is comparable to solar heating rates, gravity waves are unlikely to dominate the energetics of the thermosphere. Their main contribution should be to the dynamics of the thermospheres, through the momentum deposited in the background atmosphere. Similar behavior is seen in the Earth's lower thermosphere and may play a role also on Venus and Mars. The main significance of waves lies in transport of energy, and hence redistribution, rather than simple heating.

4. Horizontal Structures in the Atmosphere

[62] The density profiles observed by INMS (Figure 2) differ on the inbound and outbound legs of any given flyby and in addition we found the densities at T5 to be roughly a factor of 2 smaller than those at TA. As shown in Figure 1, the two flybys covered different latitudes and local times on Titan, so the obvious question is whether the measured trends could be a signatures of large-scale horizontal structures in Titan's thermosphere.

4.1. Density and Temperatures

[63] We previously in section 2.5.2 found that the the point of 1800 SLT local time and 1316 km altitude was sampled both at the TA and T5 flybys, but at different latitudes of 41.2°N and 69.1°N, respectively. The densities we found, $\rho(TA) = 6.96 \times 10^{-12}$ kg/m^3 and $\rho(T5) = 3.56 \times 10^{-12}$ kg/m^3, differed by a ratio of $\rho(TA)/\rho(T5) \approx 2$, implying significantly lower densities at higher latitudes in Titan's thermosphere. We can constrain latitudinal variations better by using all of our measurements.

[64] The difficulty with comparing data taken at any point along Cassini's flyby trajectory (and hence location in Titan's atmosphere) is that altitude changes will dominate the signatures. In order to avoid this limitation, we will instead investigate normalized densities. We produce a "standard atmosphere" from our 1-D diffusion model (described in section 2.3) and normalize our measurements to that theoretical profile. The obtained normalized densities ρ_{norm} are defined as $\rho_{norm} = \rho_{obs}/\rho_{fit}$, where ρ_{obs} and ρ_{fit} are mass densities derived from our observations and given by the 1-D diffusion model model, respectively. As described in section 2.3 and shown in Figure 2, our modeled best fit atmosphere profiles differed for the TA and T5 flybys. Since our purpose now is to compare measurements from both flybys, we need a common "standard atmosphere." While this could in principle be either of the two, we defined our best fit atmosphere density values ρ_{fit} at each altitude as the log-linear interpolation between the TA and T5 background atmosphere values.

[65] In Figure 11 we show normalized densities ρ_{norm} from TA and T5 versus latitude of the spacecraft along its trajectories (upper panel) and solar local time (bottom panel). Blue (black) and red (gray) markers denote inbound and outbound values, respectively. Green (black) markers are the densities with local time trends removed, described below. We see that our TA and T5 observations covered a wide range of latitudes reaching from around 28°N to 76°N with a gap between around 42°N and 49°N.

[66] As can be seen in the upper panel of Figure 11, a trend is apparent with densities decreasing towards higher latitudes. While we had previously described this trend for a particular pair of measurement points only (Section 2.5.2), we see here that it is consistent along Cassini's entire trajectory. Removing local time trends (green/black markers) does not greatly affect this trend. The solid and dashed line in the figure is a cosine curve fit through the measurements. This fit suggests that densities in Titan's thermosphere decrease by a factor of ~3 from 30°N to 70°N. If extrapolated to the equator this would imply equatorial densities larger by a factor of ~3.6 than values at 70°N. Note that we do not consider the polynomial fits discussed in section 2.4 in these discussions, but extracted these horizontal trends independently. Since all measurements presented here are for the northern hemisphere, we currently cannot constrain the shape of Titan's atmosphere in the southern hemisphere.

[67] The blue (black) and red (gray) values plotted in the upper panel of Figure 11 may also include local time and longitude structures. In an attempt to separate the latitude and local time variations, we show in the bottom panel of Figure 11 the same values, but as a function of solar local time of the spacecraft on its trajectories. As a result of the latitude trend, T5 values in the bottom panel of Figure 11 are smaller than the TA values and shifted vertically. We hence extracted the latitudinal trend from the observations and show the resulting densities with green (black) symbols in the bottom panel. With latitudinal trends removed, TA and T5 data in the local time space form an almost continuous data set from around 15 hours SLT to 2 hours SLT, or almost half a Titan day centered around 21 hours SLT. Between 18 hours and 0 hours SLT the values show no clear trend, but densities decrease before 18 hours and after midnight. The solid line is a simple diurnal sinusoid fit to the data which suggests a peak in densities toward 21 hours SLT. Since no information is available for the early morning and daytime densities, we cannot currently determine whether the minimum near 09 hours SLT suggested by our fit is real.

[68] The solid lines in both panels of Figure 11 hence represent possible horizontal structures of mass density in Titan's thermosphere. The latitudinal gradient appears better constrained than the local time behavior, in particular in terms of the magnitude of the horizontal variations. Across our data sets from TA and T5 the densities vary by around 50% with local time, but it is unclear whether this represents a diurnal amplitude or less. This uncertainty is indicated in the bottom panel of Figure 11 through the dashed lines. Also, it is apparent that the variation may not be a simple diurnal sinusoid, but in the absence of any further evidence this is a plausible first guess. In deriving the latitude and local time structures we have assumed that Titan's atmo-
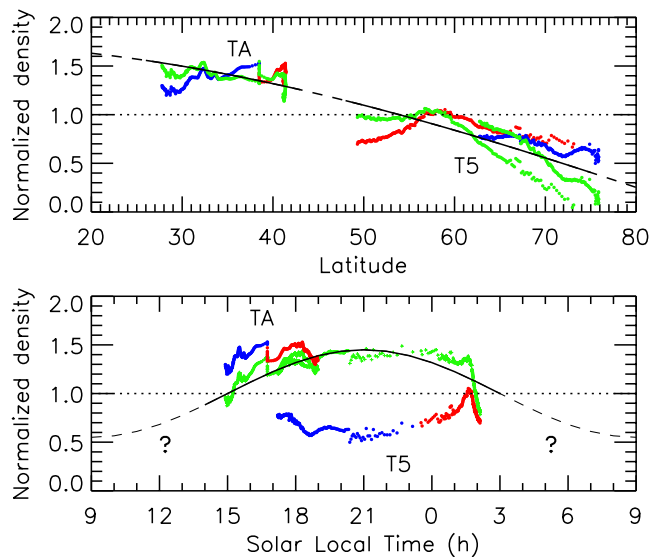

Figure 11. Normalized mass densities in Titan's thermosphere based on the INMS measurements during the TA and T5 flybys, mapped versus latitude (upper panel) and solar local time (bottom panel). The values have been normalized to a vertical density profile from a diffusion model, thereby removing altitude variations. Blue and red (gray) markers denote values measured during inbound and outbound passes, respectively. Solid lines are cosine fits through the data points which indicate possible latitude and local time trends of the densities. Green (black) markers in the upper panel are normalized densities with their local time trends removed. Green (black) markers in the bottom panel are normalized densities with their latitude trends removed.

sphere did not significantly change between the TA and T5 flybys. Large temporal variations, if present, could partly invalidate our results. Analysis of multiple future Titan flybys over the course of the Cassini mission will allow us to better separate temporal and latitudinal variations.

[69] The observed local time behavior of densities suggests that thermospheric temperatures on Titan peak near dusk. If one considers solar EUV heating as the main energy source in Titan's thermosphere, the maximum temperature is reached within a few hours SLT of local noon [*Müller-Wodarg et al.*, 2000, 2003], slightly offset from the subsolar point due to a complex interplay of composition variations, adiabatic processes and solar EUV heating. Our observations differ considerably from this solar-driven case, suggesting either the presence of important other energy sources on Titan or the presence of external momentum sources which affect the winds, shifting the temperature extrema. Calculations by *Müller-Wodarg et al.* [2000] showed that prograde superrotation of Titan's thermosphere could shift the temperature maximum towards the dusk sector. We will discuss thermospheric superrotation in section 4.3.

[70] Our isothermal fits to the TA and T5 densities (section 2.3) suggested temperatures larger by ~5 K during T5. This may in part be manifestation of a local time variation, with T5 measurements being centered around the evening sector, if indeed temperatures exhibit the local time variations suggested by the densities in Figure 11. We

also carried out isothermal fits separately for the inbound and outbound densities during any given flyby and found outbound temperatures during TA larger by 2–3 K and those at T5 smaller by an equal amount with respect to the inbound values. This again supports the notion of an early evening temperature maximum in Titan's thermosphere.

[71] Observations by the Pioneer Venus Orbiter spacecraft revealed strong horizontal variations of thermospheric density on Venus. Atmospheric drag and mass spectrometer measurements showed that densities near 150 km on Venus decreased by around an order of magnitude from equator to pole and by roughly the same amount with local time [*Niemann et al.*, 1980; *Keating et al.*, 1985]. Equatorial densities are largest over the equator on the dayside and smaller than the polar densities on the nightside. While our observations generally suggest larger equatorial densities, they were mostly carried out on the late afternoon to midnight sector, so the structure on Titan may be more complicated, resembling more that of Venus, but with additional seasonal effects. More observations are needed to determine this.

4.2. Horizontal Variations of CH_4

[72] While our discussions so far addressed horizontal variations of total mass density in Titan's thermosphere, we will finally examine to what extent composition varies horizontally. As previously noted, calculations by *Müller-Wodarg et al.* [2003] suggested considerable local time and latitude variations of CH_4 abundances, which were in their model driven by the global circulation. Do we find evidence of similar variations in the INMS observations?

[73] Figure 12 shows mole fractions of CH_4 during the TA and T5 flybys. The upper panel shows values plotted versus altitude, while the lower panel displays the values versus atmospheric pressure. We derived pressures in Titan's thermosphere using the procedures described in section 2.5. The dots denote TA values, while diamonds denote T5 values. Blue (black) symbols are inbound mole fractions, red (gray) symbols are outbound. Also shown in Figure 12 are best fit model profiles, described in section 2.3. Solid lines are for the model fit to TA observations, dashed lines denote the T5 best fit.

[74] A clear difference is evident in the CH_4 mixing ratios during TA and T5 in the upper panel of Figure 12. Near 1400 km, the average value is around 0.07 during TA and 0.10 during T5. However, when plotting these versus pressure (bottom panel), the differences between TA and T5 reduce to less than 0.01 at any pressure level. Consistently in both flybys, outbound mixing ratios are larger than inbound values by up to ∼0.03.

[75] With CH_4 being the lighter gas in our height regime, its mole fraction increases with altitude. When sampling at a given altitude a lower pressure regime we therefore encounter a larger mole fraction of CH_4. This effect is purely due to atmospheric expansion and does not constitute a real change in composition. When examining composition on isobaric surfaces, we compensate for any atmospheric expansion effects. The finding that CH_4 mixing ratios agree very well between TA and T5 when plotted versus pressure suggests that the differences found at fixed altitudes (upper panel) are caused by the atmosphere at TA being more expanded that at T5. In terms of isobaric surfaces, we are during T5
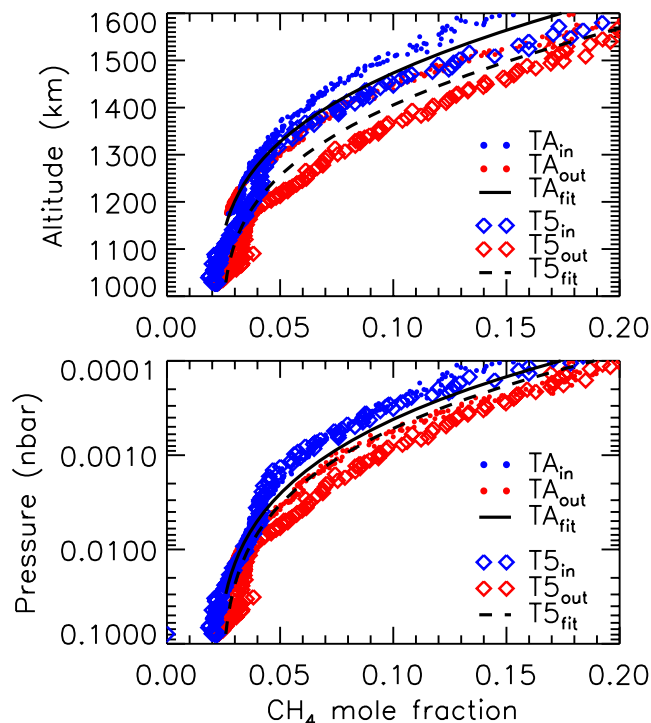

Figure 12. Mole fractions of CH_4 in Titan's thermosphere, as measured by Cassini's INMS during the TA and T5 flybys. The upper panel shows values plotted versus altitude, the bottom panel shows them versus pressure. Blue (black) markers denote inbound measurements, red (gray) markers are outbound. Black lines are best fits from our 1-dimensional diffusion model for TA (solid) and T5 (dashed) conditions.

sampling a lower pressure region in the atmosphere than at TA, and it is this which causes the main difference in CH_4 densities during TA and T5.

[76] Interestingly, differences between inbound and outbound CH_4 mole fractions persist on isobars (bottom panel of Figure 12), suggesting a departure from diffusive equilibrium. Differences are generally smaller during TA (dots) than T5 (diamonds) and reach up to 50% near the top of our altitude and pressure range. This value is consistent with local time changes in CH_4 mole fractions found in the calculations by *Müller-Wodarg et al.* [2003]. Equally, the fact that mole fractions appear to be enhanced towards Titan's nightside (comparing T5 inbound and outbound) is consistent with their calculations, which found an enhancement of CH_4 abundances due to subsistence of the atmosphere at night. This, however, needs to be examined also in context with the local time structure of temperatures, which we found to possibly differ between the model and observations (see section 4.1). We will address this in more detail in a separate study.

4.3. Thermospheric Winds

[77] In the following, we will use the horizontal density structures inferred from INMS measurements to estimate zonal wind speeds in Titan's thermosphere. Following

Holton [1992], the thermospheric zonal winds in steady state conditions satisfy the relation

$$u^2 \tan(\theta) = -\frac{1}{\rho}\frac{1}{a}\frac{\partial p}{\partial \theta} + 2\,\Omega\,u \sin(\theta) \qquad (9)$$

where u are the eastward wind velocities, θ the latitude, a the distance to Titan's center, p the atmospheric pressure and Ω is Titan's rotation period. The equation gives a relation between zonal winds and latitudinal pressure gradients. From the ideal gas law we have

$$\frac{\Delta p}{\rho} \approx \frac{RT}{M}\frac{\Delta \rho}{\rho} \qquad (10)$$

where R is the universal gas constant, T the temperature and M the mean molecular mass. We may integrate both sides of equation 9 between latitudes $\theta = 40°–60°$ and obtain with equation 10, assuming $T = 150$ K and $M = 27$, an expression relating u (in ms^{-1}) to normalized density changes $\Delta\rho/\rho$ between $40°$ and $60°$ latitude:

$$0.43\,u^2 = -46185\left[\frac{\Delta\rho}{\rho}\right]_{40}^{60} + 9.64\,u \qquad (11)$$

From Figure 11 we see that $[\Delta\rho/\rho]_{40}^{60} \approx -0.5 \pm 0.2$. Solution of equation (11) then gives zonal wind speeds of $u \approx 245 \pm 50$ ms^{-1}. The sound speed in Titan's thermosphere is $c \approx 255$ ms^{-1}, so the derived zonal wind speeds appear to be close to the sound speed. Given the number of approximations made in this simple calculation the derived zonal wind speed should be regarded as rough value. It appears from these calculations that Titan's thermosphere, similar to its stratosphere [*Hubbard et al.*, 1993; *Moreno et al.*, 2005; *Sicardy et al.*, 2006], may be superrotating.

5. Discussion and Conclusions

[78] Using in situ observations of neutral gas densities by the INMS instrument on board Cassini, we have identified vertically propagating waves and horizontal structures in Titan's thermosphere above around 1000 km altitude. Average vertical wavelengths ranged from 170 to 360 km and amplitudes in density from 4 to 12%, in temperature from 4 to 7 K for individual wave trains or 5–10 K in total. Inferred wave periods, without considering effects of doppler-shifting by background winds, are in the order of hours. We estimated that damping of these waves by viscosity and conduction could lead to considerable acceleration and possibly vertical redistribution of energy in Titan's thermosphere. This suggests that Titan's thermosphere, like those of Earth, Mars, Venus and the Gas Giants, is strongly influenced by the atmosphere below through dynamical coupling.

[79] The problem of separating wave signatures from larger scale background trends in the atmosphere as well as identifying background trends from one flyby alone proved very challenging and we hence combined observations from both flybys. These occurred 6 months apart, when Titan was at a different position in Saturn's magnetosphere, which along with changes in solar radiation may have influenced the global temperatures and composition on Titan, an effect that we did not address in this study. If present, such temporal variations could partly invalidate our findings on horizontal

structures, an issue we can only assess by analyzing further future Titan flybys by Cassini. We also did not address the issue of longitudinal structures, which may give important clues about global wave structures, but would need more observations to be reliable. Despite these shortcomings we were able to infer some key properties of the waves and horizontal density structures in Titan's thermosphere. The inferred local time behavior of temperatures, although still tentative, suggests that Titan's thermal structure cannot be fully understood by considering solar heating as the primary source of energy and momentum. Either other energy sources, such as magnetospheric heating, play a role and influence the local time structure, or we are observing the effects of advection. Calculations with the General Circulation Model by *Müller-Wodarg et al.* [2000] have shown that prograde superrotation of Titan's thermosphere would shift the dayside temperature maximum towards the dusk sector. The inferred temperature behavior thus supports the possibility of superrotation occurring in Titan's thermosphere.

[80] Owing to the limited sampling height range we could not accurately determine the frequencies of the observed waves, and hence we can only speculate about their origins at this point. The recent study by *Strobel* [2006] suggested that gravitational tides could play an important role in Titan's thermosphere. Our measured vertical wavelengths and amplitudes are broadly consistent with the gravitational tides calculated by *Strobel* [2006], but we showed that damping by molecular viscosity and conduction could prevent waves with periods of more than several hours from reaching the thermospheric height range that we sampled. Some uncertainty remains in this value since background winds can Doppler-shift the wave periods, possibly allowing longer period waves to propagate to higher altitudes. This will be investigated in a separate study once better constraints are available on thermospheric winds. Solar tides, which are important on Earth, do not play a significant role on Titan compared with the gravitational tides due to Titan's large distance from the Sun.

[81] An important result from our study was the latitudinal structure of densities in Titan's thermosphere, which suggested the atmosphere to be expanded at towards equatorial latitudes. The factor of $3-4$ increase of densities from pole to equator is consistent with an isobar near 1400 km being located around 120 km higher in altitude near the equator than at polar latitudes. From this latitudinal density gradient we inferred zonal wind speeds in Titan's thermosphere of the order of 245 ± 50 ms^{-1}, which are close to the sound speed. Wind speeds of the order of $60-200$ ms^{-1} have been observed in Titan's stratosphere and lower mesosphere from ground-based observations [*Hubbard et al.*, 1993; *Kostiuk et al.*, 2001, 2005; *Luz et al.*, 2005; *Moreno et al.*, 2005; *Sicardy et al.*, 2006] as well as recent infrared observations by Cassini's Composite Infrared Spectrometer (CIRS) [*Flasar et al.*, 2005].

[82] From our derivation we cannot determine the direction of the thermospheric zonal winds. Direct observations of stratospheric and mesospheric winds on Titan have shown these to be prograde [*Kostiuk et al.*, 2001, 2005; *Luz et al.*, 2005; *Moreno et al.*, 2005], but that allows no conclusive statement about the thermospheric winds. Observations by *Moreno et al.* [2005] suggest a decrease of zonal wind speeds by around 100 ms^{-1} between 300 and 450 km

altitude. Momentum deposition by dissipating or breaking gravity waves can potentially deposit momentum into the atmosphere below 1000 km and alter the zonal wind speeds, even reversing their direction. The calculations by *Müller-Wodarg et al.* [2000] which assumed prograde superrotating winds and found a temperature maximum in the early evening hours, as suggested also by our observations, may lend support to the thermospheric winds being prograde, but more observational constraints are needed to determine the wind structure between around 450 and 1000 km altitude, and thereby that of the thermosphere.

[83] Calculations with a General Circulation Model have suggested that coupling of temperature, dynamics and composition are particularly effective on Titan [*Müller-Wodarg et al.*, 2003]. The implication is that we will not be able to fully understand Titan's global thermosphere if we don't understand at least two of these components. While the INMS observations presented here are an important step towards that goal, further observations are needed to better constrain the problem. We expect these to be made during Cassini's remaining nominal mission. The measurements presented here as well as future observations will be play a key role in constraining General Circulation Models which will be an important tool for better understanding the morphology of the processes shaping Titan's thermosphere.

References

Flasar, F. M., et al. (2005), Titan's atmospheric temperatures, winds, and composition, *Science*, *308*, 975–978, doi:10.1126/science.1111150.

Friedson, A. J. (1994), Gravity waves in Titan's atmosphere, *Icarus*, *109*, 40–57, doi:10.1006/icar.1994.1076.

Fulchignoni, M., et al. (2005), In situ measurements of the physical characteristics of Titan's environment, *Nature*, *438*, 785–791, doi:10.1038/nature04314.

Hickey, M. P., R. L. Walterscheid, and G. Schubert (2000), Gravity wave heating and cooling in Jupiter's thermosphere, *Icarus*, *148*, 266–281, doi:10.1006/icar.2000.6472.

Hinson, D. P., and G. L. Tyler (1983), Internal gravity waves in Titan's atmosphere observed by Voyager radio occultation, *Icarus*, *54*, 337–352, doi:10.1016/0019-1035(83)90202-6.

Holton, J. R. (1992), *An Introduction to Dynamic Meteorology*, Int. Geophys. Ser., 3rd ed., Elsevier, New York.

Hubbard, W. B., et al. (1993), The occultation of 28 SGR by Titan, *Astron. Astrophys.*, *269*, 541–563.

Kasprzak, W. T., H. B. Niemann, A. E. Hedin, and S. W. Bougher (1993), Wave-like perturbations observed at low altitudes by the Pioneer Venus Orbiter Neutral Mass Spectrometer during orbiter entry, *Geophys. Res. Lett.*, *20*, 2755–2758.

Keating, G. M., J. L. Bertaux, S. W. Bougher, R. E. Dickinson, T. E. Cravens, and A. E. Hedin (1985), Models of Venus neutral upper atmosphere - Structure and composition, *Adv. Space Res.*, *5*, 117–171, doi:10.1016/0273-1177(85)90200-5.

Kostiuk, T., K. E. Fast, T. A. Livengood, T. Hewagama, J. J. Goldstein, F. Espenak, and D. Buhl (2001), Direct measurement of winds of Titan, *Geophys. Res. Lett.*, *28*, 2361–2364.

Kostiuk, T., et al. (2005), Titan's stratospheric zonal wind, temperature, and ethane abundance a year prior to Huygens insertion, *Geophys. Res. Lett.*, *32*, L22205, doi:10.1029/2005GL023897.

Luz, D., et al. (2005), Characterization of zonal winds in the stratosphere of Titan with UVES, *Icarus*, *179*, 497–510, doi:10.1016/j.icarus.2005.07.021.

Mason, E. A., and T. R. Marrero (1970), *The Diffusion of Atoms and Molecules*, vol. 6, pp. 155–232, Elsevier, New York.

Matcheva, K. I., and D. F. Strobel (1999), Heating of Jupiter's thermosphere by dissipation of gravity waves due to molecular viscosity and heat conduction, *Icarus*, *140*, 328–340, doi:10.1006/icar.1999.6151.

Moreno, R., A. Marten, and T. Hidayat (2005), Interferometric measurements of zonal winds on Titan, *Astron. Astrophys.*, *437*, 319–328, doi:10.1051/0004-6361:20042117.

Müller-Wodarg, I. C. F., and R. V. Yelle (2002), The effect of dynamics on the composition of Titan's upper atmosphere, *Geophys. Res. Lett.*, *29*(23), 2139, doi:10.1029/2002GL016100.

Müller-Wodarg, I. C. F., R. V. Yelle, M. J. Mendillo, L. A. Young, and A. D. Aylward (2000), The thermosphere of Titan simulated by a global three-dimensional time-dependent model, *J. Geophys. Res.*, *105*, 20,833–20,856.

Müller-Wodarg, I. C. F., R. V. Yelle, M. J. Mendillo, and A. D. Aylward (2003), On the global distribution of neutral gases in Titan's upper atmosphere and its effect on the thermal structure, *J. Geophys. Res.*, *108*(A12), 1453, doi:10.1029/2003JA010054.

Niemann, H. B., W. T. Kasprzak, A. E. Hedin, D. M. Hunten, and N. W. Spencer (1980), Mass spectrometric measurements of the neutral gas composition of the thermosphere and exosphere of Venus, *J. Geophys. Res.*, *85*, 7817–7827.

Reber, C. A., A. E. Hedin, D. T. Pelz, L. H. Brace, and W. E. Potter (1975), Phase and amplitude relationships of wave structure observed in the lower thermosphere, *J. Geophys. Res.*, *80*, 4576–4580.

Sicardy, B., et al. (1999), The structure of Titan's stratosphere from the 28 Sgr occultation, *Icarus*, *142*, 357–390, doi:10.1006/icar.1999.6219.

Sicardy, B., et al. (2006), The two Titan stellar occultations of 14 November 2003, *J. Geophys. Res.*, *111*, E11S91, doi:10.1029/2005JE002624.

Smith, G. R., D. F. Strobel, A. L. Broadfoot, B. R. Sandel, D. E. Shemansky, and J. B. Holberg (1982), Titan's upper atmosphere - Composition and temperature from the EUV solar occultation results, *J. Geophys. Res.*, *87*, 1351–1359.

Strobel, D. F. (2002), Aeronomic systems on planets, moons, and comets, in *Comparative Atmospheres in the Solar System*, edited by M. Mendillo, A. Nagy, and J. H. Waite, pp. 7–22, AGU, Washington, D. C.

Strobel, D. F. (2006), Gravitational tidal waves in Titan's upper atmosphere, *Icarus*, *182*, 251–258, doi:10.1016/j.icarus.2005.12.015.

Strobel, D. F., M. E. Summers, and X. Zhu (1992), Titan's upper atmosphere - Structure and ultraviolet emissions, *Icarus*, *100*, 512–526, doi:10.1016/0019-1035(92)90114-M.

Tokano, T., and F. M. Neubauer (2002), Tidal winds on Titan caused by Saturn, *Icarus*, *158*, 499–515, doi:10.1006/icar.2002.6883.

Vervack, R. J., B. R. Sandel, and D. F. Strobel (2004), New perspectives on Titan's upper atmosphere from a reanalysis of the Voyager 1 UVS solar occultations, *Icarus*, *170*, 91–112, doi:10.1016/j.icarus.2004.03.005.

Waite, J. H., et al. (2004), The Cassini Ion and Neutral Mass Spectrometer (INMS) Investigation, *Space Sci. Rev.*, *114*, 113–231, doi:10.1007/s11214-004-1408-2.

Waite, J. H., et al. (2005), Ion Neutral Mass Spectrometer results from the first flyby of Titan, *Science*, *308*, 982–986, doi:10.1126/science.1110652.

Yelle, R. V., and S. Miller (2004), Jupiter's thermosphere and ionosphere, in *Jupiter: The Planet, Satellites and Magnetosphere*, edited by F. Bagenal, T. E. Dowling, and W. B. McKinnon, pp. 185–218, Cambridge Univ. Press, New York.

Yelle, R. V., D. F. Strobell, E. Lellouch, and D. Gautier (1997), Engineering models for Titan's atmosphere, in *Huygens: Science, Payload and Mission*, edited by A. Wilson, *Eur. Space Agency Spec. Publ.*, ESA SP-1177, 243–256.

Yelle, R. V., N. Borggren, V. de La Haye, W. T. Kasprzak, H. B. Niemann, I. Müller-Wodarg, and J. H. Waite (2006), The vertical structure of Titan's upper atmosphere from Cassini Ion Neutral Mass Spectrometer measurements, *Icarus*, *182*, 567–576, doi:10.1016/j.icarus.2005.10.029.

Young, L. A., R. V. Yelle, R. Young, A. Seiff, and D. B. Kirk (1997), Gravity waves in Jupiter's thermosphere, *Science*, *267*, 108–111.

———————————

N. Borggren and R. V. Yelle, Lunar and Planetary Laboratory, University of Arizona, Tucson, AZ 85721, USA. (yelle@lpl.arizona.edu)

I. C. F. Müller-Wodarg, Space and Atmospheric Physics Group, Imperial College London, Prince Consort Road, London SW7 2BW, UK. (i.muellerwodarg@imperial.ac.uk)

J. H. Waite Jr., Southwest Research Institute, 6220 Culebra, San Antonio, TX 78228-0510, USA. (hwaite@swri.edu)